

# Design and Characterization of a Power Transfer Inductive Link for Wireless Sensor Network Nodes

R. W. Porto, V. J. Brusamarello, I. Müller

Electrical Engineering Department

Universidade Federal do Rio Grande do Sul

Porto Alegre, RS, Brazil

{wolff.porto, valner.brusamarello, ivan.muller}@ufrgs.br

F. R. de Sousa

Electrical Engineering Department

Universidade Federal de Santa Catarina

Florianópolis, SC, Brazil

rangel@ieec.org

**Abstract**—This paper describes a design of a power transfer inductive link for charging batteries of wireless sensor network nodes. The application physical constraints imposes a maximum size for the coils and demands a design methodology to maximize output power delivered to the load and energy transmission efficiency. This paper presents a complete methodology for designing the coils of wireless power transfer systems applied to rechargeable batteries of wireless sensor network nodes. The design of an inductive link is presented as a case study, in which two planar coils are built in order to validate the proposed method. Moreover, a complete wireless power transfer system is developed for the proposal, including coils, primary power source, capacitor network compensation, and secondary power management, with rectification, filtering, regulation, and battery charge control. The experimental results for working distances between the coils from 1 mm to 10 mm are reported as well as the frequency response of the entire system.

**Index Terms**—Inductive link; Electromagnetic coupling; Mutual inductance; Wireless power transfer.

## I. INTRODUCTION

Wireless power transfer is a technique to transfer energy to remote devices. It has been used in several application such as biomedical implants [1]-[4], radiofrequency identification [5], [6] and consumer electronics in charging pads for mobile devices [7]. This technique is also used for high power applications such as charging electric vehicles [8]-[9]. Although the constraints of applications are naturally different, it is still possible to establish a procedure for the design of the inductive link in different practical situations [10].

One important application that can take advantage from wireless power transfer is wireless sensor networks (WSN). Most of the WSN applications uses nodes that are usually powered by primary battery cells, due to very low power consumption that extends battery life up to its own endurance, i.e., they can last up to its operational life. Therefore, there is no need of secondary cells (rechargeable) and their management circuits. However, there are some situations where a rechargeable sensor node is a better choice: (i) when a sensor node is part of a WSN development tool, employed to evaluate routing protocols, sensing techniques, and other important details before the final product development; (ii) when a sensor

node is a sealed device, used in harsh environments such as a floating device to monitor water quality; (iii) when energy harvesting is used to recharge a batteryless device, using a supercap as reservoir.

Another important characteristic of wireless battery recharging system is the power transfer efficiency, which plays an important role in overall performance. High efficiency allows reducing the size of external power source and heat dissipation [11], which is a desirable feature for small devices such as WSN nodes.

In this work, a wireless power transfer system is developed for a WSN node that has been employed in several applications, some of them requiring sealed devices. The charging circuitry of the application requires a minimum input voltage of 5 VDC and an input current above 100 mA. A block diagram of the proposed inductive link is presented in Fig. 1. The inductive link is designed for operating at 500 kHz and distance between coils of 3 mm. The experimental and simulation results have shown that the presence of rectifier and filter capacitor at the system's output do not affect significantly the resonant frequency of the link. Thus, the entire load can be modeled as a single resistive load.

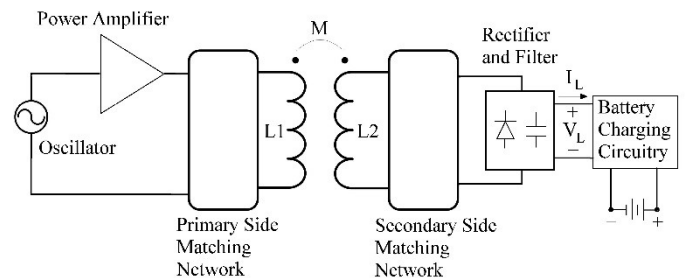


Figure 1. Block diagram of the proposed inductive link.

## II. INDUCTIVE LINK MODELING

The wireless power transfer is carried out by two magnetically coupled coils, which are usually represented by two inductances,  $L_1$  (primary coil) and  $L_2$  (secondary coil), and a mutual inductance  $M$ , as shown in Fig. 1. In order to compensate the inductive reactance of the link and to improve

the power delivered to the load, a capacitor network is placed between the voltage source and primary coil, and another capacitor network is placed between the secondary coil and the load. In [12], it was presented the full four capacitor compensation circuit. This topology is attractive, because the degrees of freedom introduced by four capacitors allows fine-tune of the resonant circuit, maximizing the power transfer from the source to the load. In addition, one can control the working frequency in order to compensate the discrete nature of these electronic components, for example the preferred value system of Electronic Industries Association (EIA). The inductive link compensated with four capacitors is presented in Fig. 2.

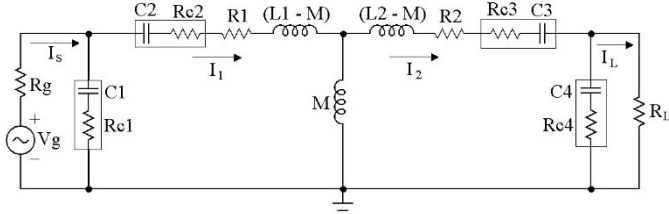


Figure 2. Equivalent T circuit of inductive link compensated with the capacitive network, where  $R_1$  and  $R_2$  are the series equivalent resistances of primary and secondary coils, respectively,  $R_g$  is the output resistance of the voltage source  $V_g$ , and  $R_L$  is the load resistance.  $R_c$  is the equivalent series resistance of each capacitor.

The mutual inductance  $M$  is defined by:

$$M = k \cdot \sqrt{L_1 \cdot L_2} \quad (1)$$

Where  $k$  is the coupling coefficient.

The mesh equations that represent the circuit in Fig. 2 can be written as a linear equations system, according to (2).

$$\begin{cases} \left( R_g + R_{c1} - \frac{j}{\omega C_1} \right) I_s - \left( R_{c1} - \frac{j}{\omega C_1} \right) I_1 = V_g \\ - \left( R_{c1} - \frac{j}{\omega C_1} \right) I_s + \left( R_{c1} - \frac{j}{\omega C_1} + R_{c2} - \frac{j}{\omega C_2} + R_1 + j\omega L_1 \right) I_1 - j\omega M \cdot I_2 = 0 \\ - j\omega M \cdot I_1 + \left( R_2 + j\omega L_2 + R_{c3} - \frac{j}{\omega C_3} + R_{c4} - \frac{j}{\omega C_4} \right) I_2 - \left( R_{c4} - \frac{j}{\omega C_4} \right) I_L = 0 \\ - \left( R_{c4} - \frac{j}{\omega C_4} \right) I_2 + \left( R_{c4} - \frac{j}{\omega C_4} + R_L \right) I_L = 0 \end{cases} \quad (2)$$

The linear system can be solved for output current  $I_L$  and the result is:

$$I_L = \frac{Z_{c1} \cdot Z_{c2} \cdot X_M \cdot V_g}{A(R_g + Z_{c1})[B(Z_{c4} + R_L) - Z_{c4}^2]} \quad (3)$$

$$\text{Where, } A = Z_{c1} + Z_{c2} + Z_{L1} - \frac{Z_{c1}^2}{(R_g + Z_{c1})}, \quad (4)$$

$$B = Z_{L2} + Z_{c3} + Z_{c4} - X_M^2 \cdot A^{-1}, \quad (5)$$

and  $Z_{c1} = R_{c1} - j/\omega C_1$ ,  $Z_{c2} = R_{c2} - j/\omega C_2$ ,  $Z_{c3} = R_{c3} - j/\omega C_3$ ,  $Z_{c4} = R_{c4} - j/\omega C_4$ ,  $X_M = j\omega M$ ,  $Z_{L1} = R_1 + j\omega L_1$ ,  $Z_{L2} = R_2 + j\omega L_2$ .

The output power  $P_o$  on the load  $R_L$  can be calculated according to:

$$P_o = \frac{1}{2} |I_L|^2 \cdot R_L \quad (6)$$

One should notice that the coupling coefficient  $k$  plays an important role for the output power of an inductive link. If we consider (1), (3) and (6) we shall see that  $P_o$  depends on  $k^2$ . In previous work [10], for a pair of planar spiral coils which are parallel and aligned, it was shown that the mutual inductance and the coupling coefficient decay with the distance as depicted in Fig. 3. Thus,  $P_o$  is highly dependent with the distance between coils for a fixed working frequency.

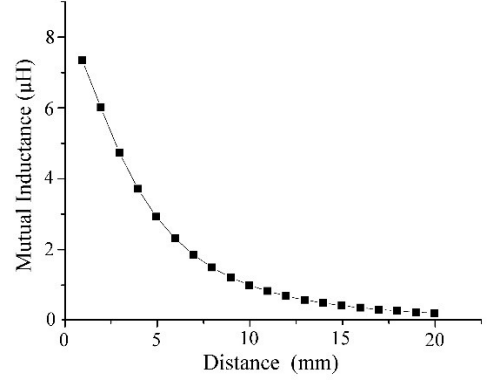


Figure 3. Mutual inductance as a function of distance between the coils' centers [10].

#### A. Planar Spiral Coil Model

There are several closed-form equations in literature to estimate the self-inductance of a coil [13]-[15]. For planar circular coils, the self-inductance can be estimated by:

$$L = \frac{\mu \cdot N^2 \cdot D_{avg}}{2} \cdot \left[ \ln \left( \frac{2.46}{\phi} \right) + 0.20 \cdot \phi^2 \right] \quad (7)$$

Where  $N$  is the number of turns,  $D_{avg}$  is the average diameter and  $\phi$  is the occupancy ratio which is calculated by:

$$\phi = \frac{D_o - D_i}{D_o + D_i} \quad (8)$$

Where  $D_o$  is the external diameter and  $D_i$  the internal diameter as illustrated in Fig. 4.

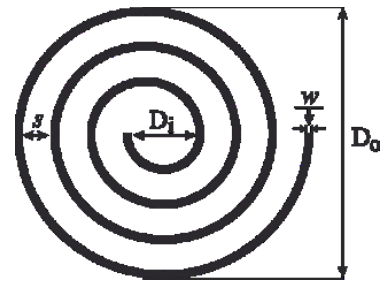


Figure 4. Typical planar circular coil and its geometric parameters [10].

In order to complete the equivalent circuit model of the coil, the series resistance and the total parasitic capacitance have to

be calculated. The series resistance under direct current,  $R_{dc}$ , is calculated by:

$$R_{dc} = \rho \cdot \frac{l}{w \cdot h} \quad (9)$$

Where  $\rho$  is the electrical resistivity,  $w$  is the width,  $h$  is the thickness, and  $l$  is the length of the conductor, which is calculated by:

$$l = \int_0^{2\pi N} \sqrt{[r(\theta)]^2 + \left[\frac{d}{d\theta}r(\theta)\right]^2} d\theta \quad (10)$$

In (10),  $r(\theta)$  is the average position of the conductor as function of angle  $\theta$  in polar coordinates. The origin is taken at the center of the spiral and  $r(\theta)$  is given by:

$$r(\theta) = \frac{D_o}{2} - \frac{\theta}{2\pi} \cdot (w + s) \quad \forall \quad 0 \leq \theta \leq 2\pi N \quad (11)$$

Where  $s$  is the spacing between the traces, as illustrated in Fig. 4.

Under alternating current the electrical series resistance will be affected by skin effect if the power transfer system operates at high frequencies. Thus, (12) is used to estimate the series resistance [11].

$$R_{ac} = R_{dc} \cdot \frac{h}{\delta \cdot \left(1 - e^{-\frac{h}{\delta}}\right)} \quad (12)$$

Where  $\delta$  is the depth penetration given by:

$$\delta = \sqrt{\frac{\rho}{\pi \cdot \mu \cdot f}} \quad (13)$$

Where  $\rho$  is the electrical resistivity of the conductor,  $\mu$  is the magnetic permeability of the medium and  $f$  is the excitation frequency.

In [11] the parasitic capacitance  $C_p$  is estimated by two components:  $C_{pc}$  formed by air dielectric, and  $C_{ps}$  formed by printed circuit board substrate, as illustrated in Fig. 5. Thus, considering the length  $l$  of the conductive material used to build the coil, then the parasitic capacitance  $C_p$  can be described by:

$$C_p = C_{pc} + C_{ps} \approx (\alpha \cdot \epsilon_{rc} + \beta \cdot \epsilon_{rs}) \cdot \epsilon_0 \cdot \frac{h \cdot l}{s} \quad (14)$$

Where  $\epsilon_{rc}$  and  $\epsilon_{rs}$  are the dielectric permittivity of the air and the substrate of the printed circuit board, respectively. The constants  $\alpha$  and  $\beta$  are determined empirically [11].

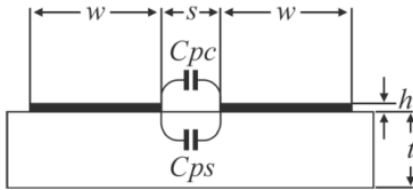


Figure 5. Cross-section of two parallel conductors and their parasitic capacitances (adapted from [11]).

## B. Mutual Inductance Calculation

The energy transmission in an inductive link is highly affected by the mutual inductance. Although derived solutions from Maxwell equations can be used for mutual inductance calculation [14]-[15], it can also be estimated by using finite elements simulation [16].

In this context, the geometry of the problem must be inserted into finite elements software as shown for instance in Fig. 6. The mutual inductance can be defined as [16]:

$$M = \frac{\phi_{2,1}}{I_1} \quad (15)$$

Where  $I_1$  is the current of the primary coil and  $\phi_{2,1}$  is the magnetic flux linking in the secondary coil due to  $I_1$ . Assuming magnetic flux in the form  $e^{j\omega t}$ , the induced voltage in the secondary coil at open circuit can be expressed as:

$$V_2 = j\omega \cdot \phi_{2,1} \quad (16)$$

Using (15) and (16), the mutual inductance can be rewritten as:

$$M = \frac{V_2}{j\omega \cdot I_1} \quad (17)$$

Alternatively, the mutual inductance can be accessed by using the coupling coefficient, which is calculated by (18). This result is used in (1) for obtaining  $M$ .

$$k = \frac{V_2}{V_1} \sqrt{\frac{R_1^2 + (\omega \cdot L_1)^2}{\omega^2 L_1 L_2}} \quad (18)$$

Where  $V_1$  is the voltage at primary side,  $V_2$  is the voltage at secondary side at open circuit, and  $L_1$  and  $L_2$  are the inductances of primary and secondary side of the link, respectively.

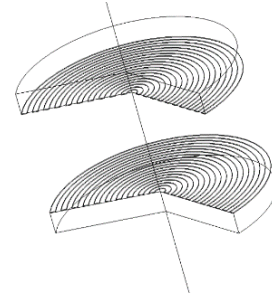


Figure 6. Example of two planar spiral coils.

If  $\omega L_1 \gg R_1$ , then (18) becomes:

$$k = \frac{V_2}{V_1} \sqrt{\frac{L_1}{L_2}} \quad (19)$$

## III. METHODOLOGY

### A. Receiver Coil Design

The geometrical parameters of secondary coil are affected by the application. In case of planar coils, one should use the full area available in order to maximize the coupling coefficient  $k$

[13]. Therefore, the internal diameter should be as small as possible and the external diameter is limited according to the maximum space available. Additionally, the fabrication technology imposes the boundaries for spacing between traces,  $s$ , and the trace's width,  $w$ . Thus, the maximum number of turns of secondary coil,  $N_2$ , is determined by these geometrical constraints. At this point, it is possible to calculate the electrical model of the secondary coil by using (7) for self-inductance,  $L_2$ , (12) for AC resistance and (14) for parasitic capacitance.

The application described in the introduction section imposes a maximum diameter of 38 mm for the receiver coil. On the other hand, the employed manufacturing process limits both spacing between traces,  $s$  and trace width,  $w$ , in 0.25 mm minimum. By using the full available area of the coil, the number of turns is  $N=38$ . The equivalent circuit of the coil is calculated with the presented equations and the results are:  $L_2 = 18.96 \mu\text{H}$ ,  $R_2 = 4.39 \Omega$  (DC resistance) and  $C_{p2} = 3.82 \text{ pF}$ .

### B. Transmitter Coil Design

In previous work [17], it was shown that there is an optimum value for the external diameter of the transmitter coil for a given distance between coils ( $z$ ). As the distance  $z$  can be at the interval 3 mm to 5 mm, for to the application under consideration, the external diameter of the transmitter coil is set to 41 mm, which is optimized for  $z = 5 \text{ mm}$ . By using the maximum number of turns allowed by technological constraints, which is  $N_1 = 41$ , the electrical model of the transmitter coil is obtained. The equivalent circuit is calculated with the presented equations and the results are:  $L_1 = 23.82 \mu\text{H}$ ,  $R_1 = 5.11 \Omega$  (DC resistance) and  $C_{p1} = 4.45 \text{ pF}$ .

### C. Mutual Inductance

As the mutual inductance depends on the geometry of the problem, a finite elements simulation was done for distances between 1 mm and 10 mm. The mutual inductance has been calculated by using (17). Specifically for  $z = 3 \text{ mm}$  and  $z = 5 \text{ mm}$ , the results were  $M = 14.36 \mu\text{H}$  ( $k = 0.67$ ) and  $M = 11.25 \mu\text{H}$  ( $k = 0.53$ ), respectively.

### D. Working Frequency Determination

The current on the load,  $I_L$ , can be calculated from the solution of the linear equations system (2), which is presented in (3), when all the parameters are considered unknown. In this case, one can notice that the power transferred to the load is a function of frequency  $P_O = f(\omega)$ . Like other circuit parameters (such as inductances and resistances losses) are fixed, the frequency can also be fixed, so that the compensation capacitors can be determined in order to maximize the power delivered to the load of this circuit in these conditions.

### E. Power Amplifier and Load Model

The wireless charging application described in this work requires a load voltage exceeding  $5 \text{ V}_{\text{DC}}$  and an output current of at least 100 mA due to battery management specifications. Thus, two types of load were considered to characterize the charging circuitry. The first one was a resistive load of  $R_L = 47 \Omega$ , which was used to determinate the capacitive compensation network. The second one was a non-linear load

made up of a bridge rectifier, a filter capacitor and the load resistor  $R_L = 47 \Omega$ .

A power amplifier was built by taking into account the output power required by the load and bandwidth for the working frequency. On should notice that the power amplifier shown in Fig. 7 has an output resistance,  $R_{g_s}$ , around  $0.5 \Omega$ .

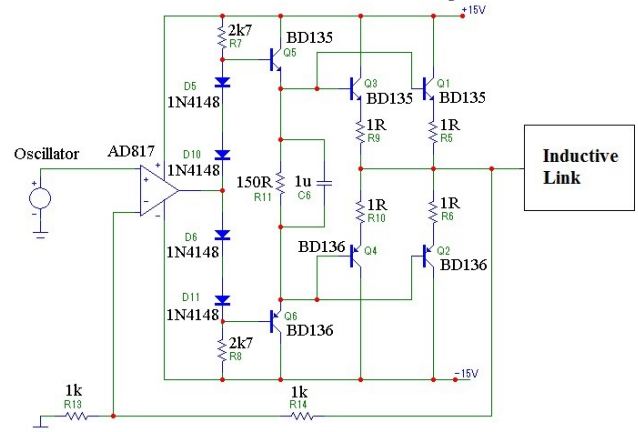


Figure 7. Power Amplifier used as a driver for the inductive link.

### F. Search Algorithm for Compensation Capacitors

It was shown in previous work [12] that the inductive link performance can be improved when compensated with a set of capacitors. Once defined the coils' model, the distance  $z$  (and consequently  $k$ ), the load  $R_L$  (considering a resistive load) and the source voltage, frequency and equivalent series resistance  $R_S$ , the search algorithm is applied to find a set of capacitors ( $C_1$ ,  $C_2$ ,  $C_3$  and  $C_4$ ) that maximizes the objective function power delivered to the load  $P_L$  or power transfer efficiency. In this case, the analytical equation of the power on the load is calculated and the set of four discrete (E24 series) capacitors with best performance are chosen and applied on the network. This process guarantees the best possible compensation choice when the rest of parameters are fixed. One should notice that the set of capacitors are chosen for one of the objective functions. Thus, for maximizing the power delivered to the load at  $z = 3 \text{ mm}$  the set of capacitors is:  $C_1 = 0.91 \text{ nF}$ ;  $C_2 = 3.6 \text{ nF}$ ,  $C_3 = 2.2 \text{ nF}$ ;  $C_4 = 300 \text{ pF}$ . If we consider a longer distance such as  $z = 5 \text{ mm}$ , the new set of capacitors will be:  $C_1 = 82 \text{ pF}$ ;  $C_2 = 5.1 \text{ nF}$ ,  $C_3 = 300 \text{ nF}$ ;  $C_4 = 2 \text{ pF}$ .

## IV. RESULTS AND DISCUSSION

The basic inductive link without capacitive compensation was evaluated by applying a sinusoidal voltage source  $V_1$  with amplitude  $20 \text{ V}_{\text{pp}}$  and frequency 500 kHz at primary coil ( $L_1$ ). A resistive load  $R_L = 47 \Omega$  was connected at secondary coil ( $L_2$ ) and the voltage amplitude  $V_2$  was measured on the load. The coils were aligned as shown in Fig. 6 and the distance between coils was varied from 1 mm to 10 mm, with a step size of 1 mm. The coupling coefficient was calculated by using (19) and the results are shown in Fig 8. The geometry of the problem was inserted into the finite elements software COMSOL Multiphysics for comparison with experimental results. As COMSOL doesn't have a special function to evaluate the mutual inductance, (17) was used to determinate the mutual inductance.

The compensated inductive link was built with the capacitors calculated for  $z = 3$  mm. The set of real capacitors was measured and we observed a variation of up to 10% of the nominal values, indicating an important source of uncertainty.

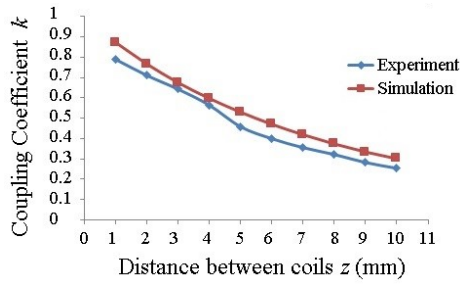


Figure 8. Coupling Coefficient as a function of distance between coils.

The first experiment was conducted with a resistive load  $R_L = 47 \Omega$  connected at the output of the link. The circuit was excited with a sinusoidal voltage source of  $20 V_{pp}$ . The AC (peak-to-peak) output voltage measurements were taken on the load for distances  $z$  between 1 mm and 10 mm, and frequencies from 100 kHz to 1 MHz. The results are shown in Fig. 9 where it can be seen the band pass behavior of the circuit. The maximum values for output voltage  $V_L$  happened at 500 kHz for distances between 1 mm and 3 mm, as it was expected. For longer distances the resonance frequency was changed to 550 kHz and it remained unchanged until  $z = 10$  mm.

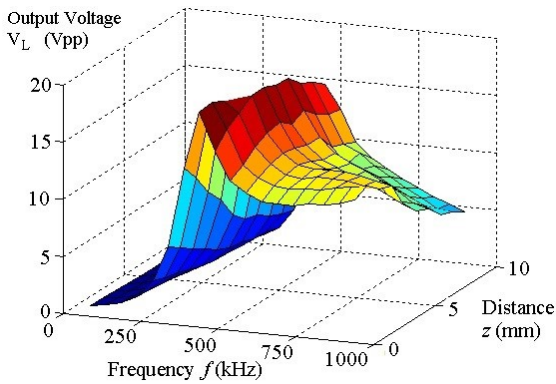


Figure 9. Output voltage measurements for compensated inductive link with resistive load.

In Fig. 10 we can observe the comparative results of output voltage measurements for two specific working distances. At distance  $z = 3$  mm, one should notice that the peak response was in 500 kHz for both simulation (theoretical equations) and experimental measurements. However, in Fig. 10 (b) the peak response of  $V_L$  was shifted to 550 kHz. The simulation results did not present this change in the frequency response.

The second experiment was carried out with the same sinusoidal voltage source of  $20 V_{pp}$ . A bridge rectifier with Schottky diodes SS14 and a following filter capacitor of 220 nF were connected at the output of the inductive link. A resistive load  $R_L = 47 \Omega$  was used in parallel of the filter capacitor. The DC output voltage measurements were taken on the load for distances  $z$  between 1 mm and 10 mm, and frequencies from 100 kHz to 1 MHz. The results are shown in Fig. 11.

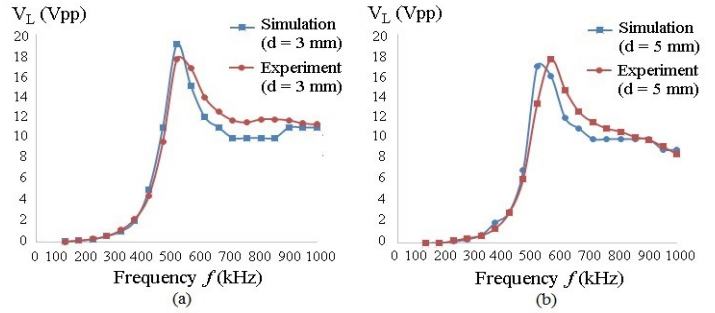


Figure 10. Output voltage measurements for a resistive load of  $47 \Omega$  as function of working frequencies for (a)  $z = 3$  mm and (b)  $z = 5$  mm.

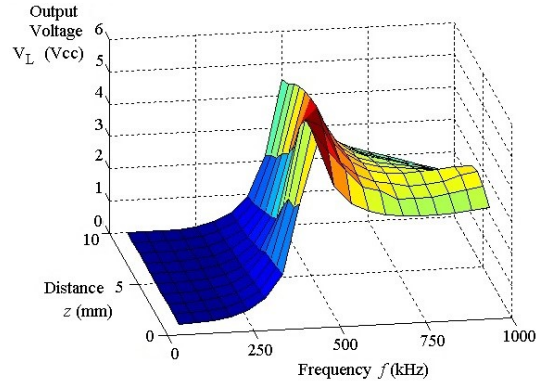


Figure 11. Output voltage measurements for compensated link with rectification and filtering.

In Fig. 12 the output voltage  $V_L$  is shown as function of frequency for the distances  $z = 3$  mm and  $z = 5$  mm. These results are similar to those presented in Fig. 10. Although the rectifier characterizes a nonlinear load, the results show that the effects introduced into the system are negligible and this load can be considered a simple resistor (in this application).

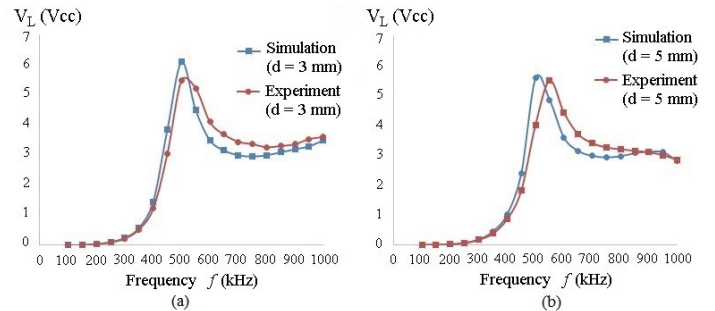


Figure 12. Output voltage measurements for inductive link with rectification and filtering and a resistive load of  $47 \Omega$  as function of working frequencies for (a)  $z = 3$  mm and (b)  $z = 5$  mm.

According to the results shown in Fig. 10 and Fig. 12, one should notice that there are two frequencies where  $V_L$  reaches the maximum value. This values are 500 kHz and 550 kHz. In Fig. 13 the output voltage  $V_L$  is shown for these two frequencies as function of the distance  $z$ . One can observe that the maximum value of  $V_L$  depends on the working frequency and distance  $z$ . If the distance is altered, the frequency should be modified for the

inductive link reach another resonant point. This happens because the mutual inductance  $M$  depends on distance  $z$  [18].

The maximum output power  $P_O$  of the circuit was 643.6 mW for  $z = 3$  mm and  $f = 500$  kHz. This result was also obtained for  $z = 5$  mm and  $f = 550$  kHz. In both cases, the output voltage  $V_L$  was above 5 VDC and output current  $I_L$  was greater than 100 mA.

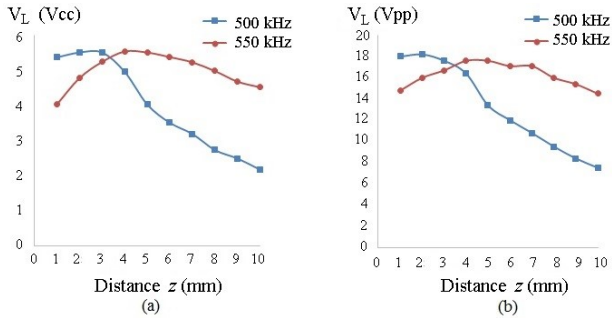


Figure 13. Output voltage measurements as a function of distance for (a) rectifier and filter capacitor in the load, and (b) with only resistive load.

## V. CONCLUSION

This paper presented the design of a wireless power transfer link for charging a wireless sensor node. The application constraints were used to design the inductive link, and thus to calculate the values of inductances from the primary and secondary coils, as well as the mutual inductance. Once defined the compensation capacitors' values by using a search algorithm described in previous work [10], one can use (3) and (6) to calculate the output power  $P_O$ .

The compensated inductive link becomes selective in terms of frequency response, as we can observe in Fig. 9 and Fig. 11. In addition, a set of compensation capacitors leads to a maximum output power for a specific working frequency and specific distance between coils. The inductive link was designed for operating in 500 kHz and  $z = 3$  mm. These results were confirmed by the experimental procedures. It was observed that the resonance frequency is significantly affected when the distance between coils is varying at distances under 3 mm (Fig. 9 and Fig. 11). If  $z$  varies, a new tuning frequency may be necessary in order to maintain the required power on the load.

Also, one can notice in Fig. 10 and Fig. 12 that the resonant frequency has not changed significantly when a full-wave rectifier and a filter capacitor was inserted between the inductive link and the resistive load. Finally, one can observe that the experimental results show that the proposed design of the inductive link fulfills the specifications imposed by the application, since the rectified and filtered output voltage  $V_L$  remains above 5 V<sub>DC</sub> for distances around  $z = 3$  mm. If the working frequency is changed to 550 kHz, the inductive link can produce  $V_L > 5$  V<sub>DC</sub> until  $z = 7$  mm.

Future works will be conducted for improving the inductive link characterization in order to investigate the change in resonant frequency as a function of distance, as well the effect

of a rectifier and filter capacitor on generic applications with generic geometries. In addition, the presented design methodology will be applied to other levels of power.

## REFERENCES

- [1] K. M. Silay, C. Dehollain, and M. Declercq, "Inductive power link for a wireless cortical implant with biocompatible packaging," in *Proc. of the IEEE Sensors Conference*, 2010, pp. 94-98.
- [2] J. C. Schuder, "Powering an artificial heart: birth of the inductively coupled-radio frequency system in 1960," *Artificial Organs*, vol. 26, no. 11, pp. 909-915, 2002.
- [3] G. M. Clark, *Cochlear Implants: Fundamentals and Applications*. New York: Springer-Verlag, 2003.
- [4] R. R. Harrison et al., "A low-power integrated circuit for a wireless 100-electrode neural recording system," *IEEE J. Solid-State Circuits*, vol. 42, no. 1, pp. 123-133, Jan. 2007.
- [5] C. Reinhold, P. Sholz, W. John, and U. Hilleringmann, "Efficient antenna design of inductive coupled RFID-systems with high power demand," *Journal of Communications*, vol. 2, no. 6, pp. 14-23, 2007.
- [6] K. Finkenzeller, *RFID-Handbook: Fundamentals and Applications in Contactless Smart Cards, Radio Frequency Identification and Near-Field Communications*, 3<sup>rd</sup> ed. John Wiley & Sons, 2010.
- [7] E. Waffenschmidt and T. Staring, "Limitation of inductive power transfer for consumer applications," *Proc. of the 13<sup>th</sup> European Conference on Power Electronics and Applications (EPE)*, 2009, pp. 1-10.
- [8] M. Budhia, G. A. Covic, and J. T. Boys, "Design and optimization of circular magnetic structures for lumped inductive power transfer systems," *IEEE Trans. on Power Electronics*, vol. 26, no. 11, pp. 3096-3108, 2011.
- [9] M. Budhia, J. T. Boys, G. A. Covic, and C. Huang, "Development of a single-sided flux magnetic coupler for electric vehicle IPT charging systems," *IEEE Trans. on Industrial Electronics*, vol. 60, no. 1, pp. 318-328, 2013.
- [10] R. W. Porto, V. J. Brusamarello, I. Müller, F. R. Sousa, and R. de Azambuja, "Design and optimization of a power inductive link," in *Instrumentation and Measurement Technology Conference (I2MTC)*, 2014 IEEE International, May. 2014, pp. 648-653.
- [11] U. M. Jow and M. Ghovanloo, "Design and optimization of printed spiral coils for efficient transcutaneous inductive power transmission," *IEEE Trans. on Biomedical Circuits and Systems*, vol. 1, no. 3, pp. 193-202, Sept. 2007.
- [12] R. de Azambuja, V. J. Brusamarello, S. Haffner, and R. W. Porto, "Analysis and optimization of na inductive power transfer with a randomized method," *IEEE Trans. on Instrumentation and Measurement*, vol. 63, no. 5, pp. 1145-1152, May. 2014.
- [13] R. Bosshard, J. Mühlethaler, J. W. Kolar, and I. Stevanovic, "Optimized magnetic design for inductive power transfer coils," *Proc. of the 28<sup>th</sup> Applied Power Electronics Conference and Exposition (APEC)*, 2013, pp. 1812-1819.
- [14] F. W. Grover, *Inductance Calculations: working formulas and tables*. Dover Publications, Inc., 1946.
- [15] W. G. Hurley, and M. C. Duffy, "Calculation of self and mutual impedances in planar magnetic structures," *IEEE Trans. on Magnetics*, vol. 31, no. 4, p. 2416-2422, July, 1995.
- [16] H. A. Ghali and H. A. Rahman, "Understanding 'Mutual Inductance' using COMSOL Multiphysics," in *Proceedings of the Comsol Conference*, Milan, 2009.
- [17] R. W. Porto, V. J. Brusamarello, I. Muller, F. R. Sousa, "A Methodology for Design and Optimization of an Inductive Power Transfer Link," Paper Submitted to *IEEE Trans. on Power Electronics*.
- [18] Brusamarello, V.J. ; Blauth, Y.B. ; de Azambuja, R. ; Muller, I. ; de Sousa, F.R. Power Transfer With an Inductive Link and Wireless Tuning, *IEEE Trans. on Instrumentation and Measurement*, Vol. 62, 2013, pp: 924-931.